**E. M. Rashad**

J. Electrical Systems 1-4 (2005): 1-16

Regular paper

Journal of Electrical Systems

# Dynamic Analysis of Series-Connected Wound Rotor Induction Motor for Variable Speed Drives

*Series-connected induction motor has the ability of operation either at two speeds; the first one is less than the synchronous speed depending on the load, while the second speed is exactly double the synchronous speed. The motor has the capability of self-starting to reach the first speed. In addition to special arrangements required to attain the second (higher) speed, instability problems have been noted in experimental operation. This paper presents a dynamic analysis of motor when supplied from a variable voltage variable frequency power supply. The starting behavior has been presented. Experimental results are given to check model validity in dynamic conditions. Then the instability problem associated with high-speed operation has been studied to investigate its reasons and suggest solutions, either in operation or in the design.*

**Keywords**: Adjustable speed drives, Motor dynamics, Stability, Wound-rotor induction motor.

## 1. INTRODUCTION

It has been proved previously that the process of electro-mechanical energy conversion is possible when the stator and rotor windings of a wound rotor induction machine are connected in series [1]. An essential requirement has to be satisfied for successful operation; the phase sequence of the rotor magneto-motive force is in the reverse sense to that of the stator. This condition can be achieved if the stator and rotor windings are properly connected. In its motoring mode, the machine can run at two speeds; the first one is less than the synchronous speed depending on the load in a similar manner to that of the conventional induction motor operation [2]. It has been shown that in this speed mode, series-connected induction motor (SCIM) has superior characteristics compared to those of conventional induction motor, especially when stator-to-rotor effective turns ratio approaches unity [3]. In the second mode of operation, SCIM runs at exactly double the synchronous speed, which is independent of the load for the stable range of operation [4]. In this mode, the motor is not capable of self-starting. A special arrangement is required to attain that high speed. For example, the motor is externally driven by another motor at no-load to the proper speed. Then the main voltage is applied to the motor. Unfortunately, in high-speed mode, experimental instability problems have

Corresponding author: emrashad@ieee.org
Department of Electrical Power and Machines Engineering,
Faculty of Engineering, Tanta University, Tanta, Egypt.

been reported [4, 5]. Both starting and instability problems have been solved satisfactorily, when vector control technique is applied [6]. However, the reasons of instability have not been explored yet.11

In this paper, dynamic behavior of SCIM is investigated for the whole speed range. The motor is supplied from variable voltage variable frequency (VVVF) supply. The starting and frequency change responses are presented with experimental verification. Then the instability problem associated with high-speed operation has been studied to investigate its reasons and suggest either operation or design solutions.

## 2. INVERTER-FED SCIM SYSTEM

The adopted drive system composes of an SCIM supplied from an inverter as VVVF supply.

### 2.1 Dynamic model of SCIM

The dynamic voltage equation of SCIM is given as follows [6]:

$$\begin{pmatrix} v_d \\ v_q \end{pmatrix} = \left( \begin{array}{c|c} R_a + L_d p & -(P/4)\omega_m L_q \\ \hline (P/4)\,\omega_m L_d & R_a + L_q p \end{array} \right) \begin{pmatrix} i_d \\ i_q \end{pmatrix} \tag{1}$$

where: $v_d = V_m \sin\delta$ , $v_q = V_m \cos\delta$

The parameters $R_a, L_d$ and $L_q$ are defined as follows:

$$R_a = R_s + R_r$$
$$L_d = L_s + L_r + \{K + (1/K) + 2\}M$$
$$L_q = L_s + L_r + \{K + (1/K) - 2\}M$$

The values of $L_s$, $L_r$, $M$ and $K$ can be obtained from the conventional tests of the machine as an induction motor. The numerical values of the employed motor parameters are given in the Appendix section.

The phase stator current is related to $i_d$ and $i_q$ according to the following relation:

$$I_a = \sqrt{\left(i_d^2 + i_q^2\right)/2} \tag{2}$$

The developed electromagnetic torque $T_e$ is given by:

$$T_e = \left(\frac{3}{2}\right)\left(\frac{P}{4}\right)\left(L_d - L_q\right) i_d i_q \tag{3}$$

The mechanical equation of motion is given by:

$$T_e - T_L = Jp\omega_m + B\omega_m \tag{4}$$

### 2.2 Inverter

A voltage source three-phase inverter has been employed in the experimental work as a VVVF power supply. The inverter is designed and manufactured by HITACHI LTD to drive a motor of 1.1 KW/1.5 HP. The technical data is as follows:

Input: 50/60 Hz, 200-240 V, 6.5 A

Output: 1-360 Hz, 200-240 V, 5 A

The inverter is provided with facilities to adjust the voltage and frequency according to a pre-determined pattern. The ratio $V_s/f_s$ is defined by the base voltage $V_{sb}$ and frequency $f_b$. For values $f_s$ less than $f_b$, the ratio is kept constant, else $V_s$ is kept at $V_{sb}$, which means flux-weakening operation. Figure 1 shows three patterns of the employed $V_s/f_s$ control. It is noted that $V_{sb}$ is 220 V. Therefore, the value of $f_b$ determines the level of $V_s/f_s$ ratio in a reverse proportion way as determined by the slope of the line.

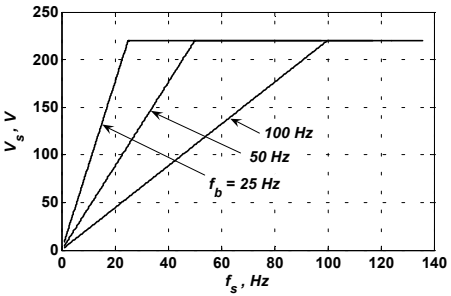


Figure 1: Inverter $V_s/f_s$ patterns for different values of base frequency $f_b$

## 3. STARTING AND FREQUENCY CHANGE RESPONSE

The dynamic model given by (1-4) has been used to compute the speed and current response for different values of supply voltage and frequency. The corresponding experimental response has been measured and digitally recorded.

### 3.1 Starting response

Figures 2, 3, 4 and 5 show the no load results when $f_b$=50 Hz for $f_s$= 15, 25, 50 and 65 Hz, respectively. The values of $f_s$ are selected to investigate both cases of constant $V_s/f_s$ and constant $V_s$. In order to check the effect of varying base

frequency, Figs. 6, 7 and 8 show the same response when $f_b$=75 Hz for $f_s$= 15, 25 and 50 Hz respectively.

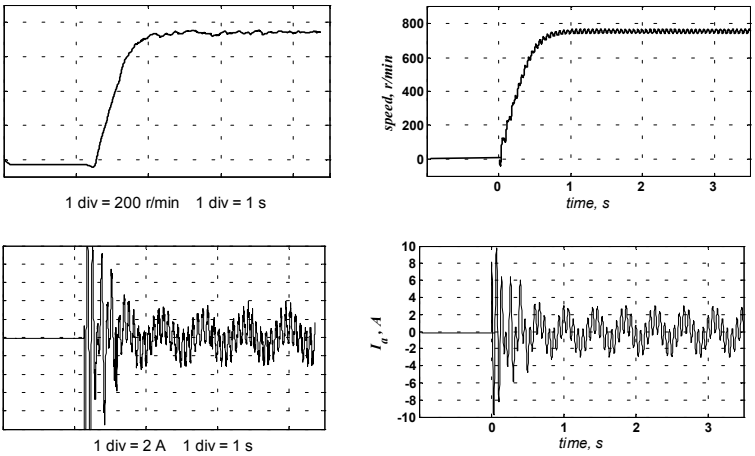


Figure 2: Starting speed (upper) and current (lower) response for $f_b$ =50 Hz and $f_s$=15 Hz at no-load.

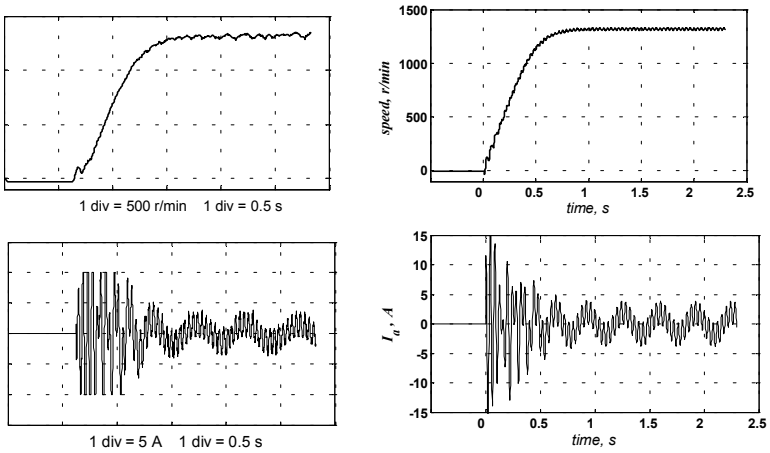


Figure 3: Starting speed (upper) and current (lower) response for $f_b$ =50 Hz and $f_s$=25 Hz at no-load.

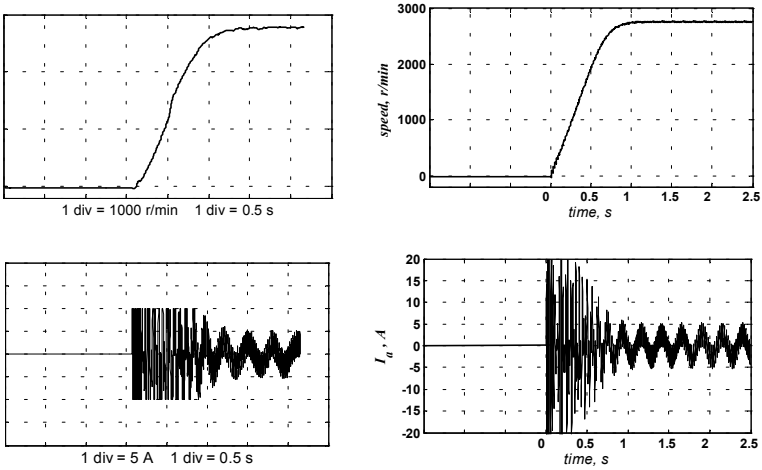


Measured Computed

Figure 4: Starting speed (upper) and current (lower) response for $f_b$ =50 Hz and $f_s$=50 Hz at no-load.

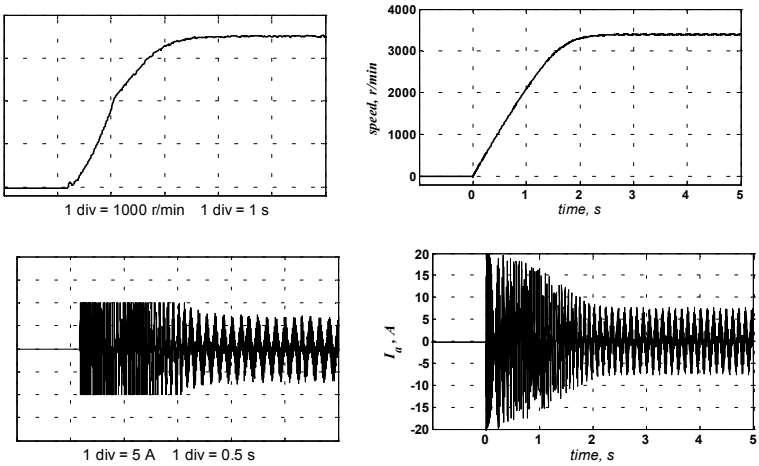


Measured Computed

Figure 5: Starting speed (upper) and current (lower) response for $f_b$ =50 Hz and $f_s$=65 Hz at no-load.

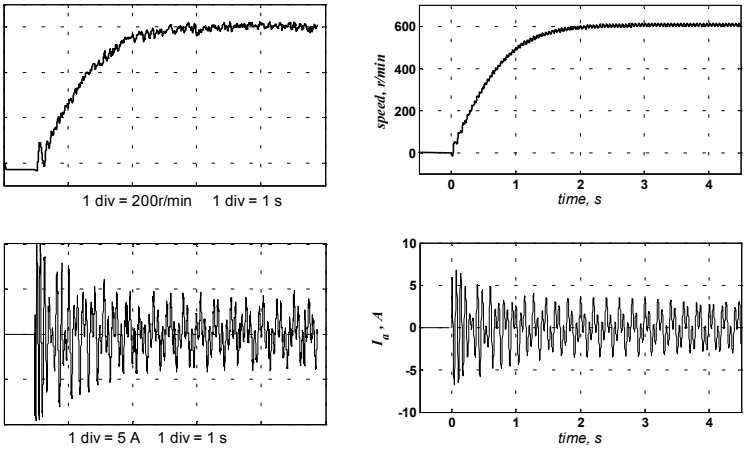


Figure 6: Starting speed (upper) and current (lower) response for $f_b$ =75 Hz and $f_s$=15 Hz at no-load.

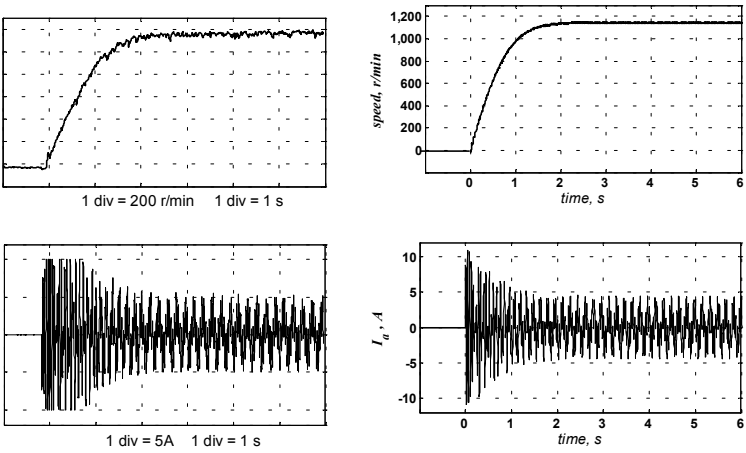


Figure 7: Starting speed (upper) and current (lower) response for $f_b$ =75 Hz and $f_s$=25 Hz at no-load.

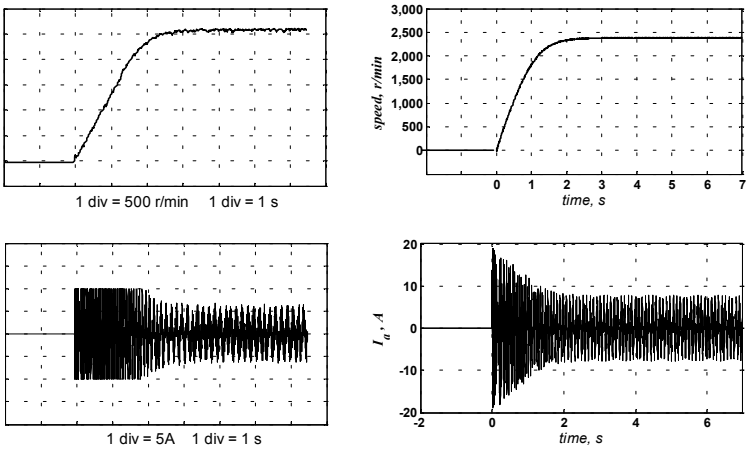


Figure 8: Starting speed (upper) and current (lower) response for $f_b$ =75 Hz and $f_s$=50 Hz at no-load.

The first note, in all cases, is that the motor starts to the low speed mode, where speed is less than the synchronous speed. From Figs. 2-4, it is noted that response speed is approximately the same for $f_s$=15, 25 and 50 Hz because of constant flux operation. The response becomes slower for $f_s$=65 Hz as shown in Figure 5. That is because the operation is at flux weakening mode, where developed torque decreases with increase in frequency. Figures 6, 7 and 8 show that the response speed is lower compared with the corresponding response in Figs. 2, 3 and 4 respectively (i.e. for the same $f_s$) in the constant flux region. This is because of the reduction in flux for higher base frequency. These observations are similar to that obtained when applying *V/f* control technique to the conventional motor types.

At steady state, all figures show the presence of current sub harmonic, which represents a feature of SCIM operation in low speed mode [3]. This sub-harmonic is at slip frequency. This means it increases with speed drop from the synchronous speed so that it can be employed to determine the motor speed. It is to be mentioned that the given measured current response is clipped when it exceeds 10 A. In this case, output voltage of the available current transducer, used in the digital recording system, exceed the voltage limit of 5 V for the data acquisition card.

### 3.2 Response to frequency change

Figure 9 shows the speed and current response to change in $f_s$ from 25 to 35 Hz for $f_b$ =50 Hz at no-load condition. Figure 10 shows the same response for load torque of 3 Nm.

The results presented in Figures 2-10 show the validity of the given dynamic model.

### 3.3 Operation at high-speed mode

The necessary arrangements to drive the motor at the high-speed mode have been prepared. The motor has been started using a dc motor and driven to the proper high speed before supply voltage is applied. Many experimental trials have been done It was not possible to get any successful operation. Once the supply voltage is applied, the motor speed decreases and operation stabilizes at the low speed mode. Moreover, the simulation dynamic program emphasizes the same notice, for a very wide range of conditions. In addition to the previously reported instability problems at high-speed mode, the failure of the adopted motor to achieve such a mode, even with low relative stability, makes it interested and important to investigate that issue.

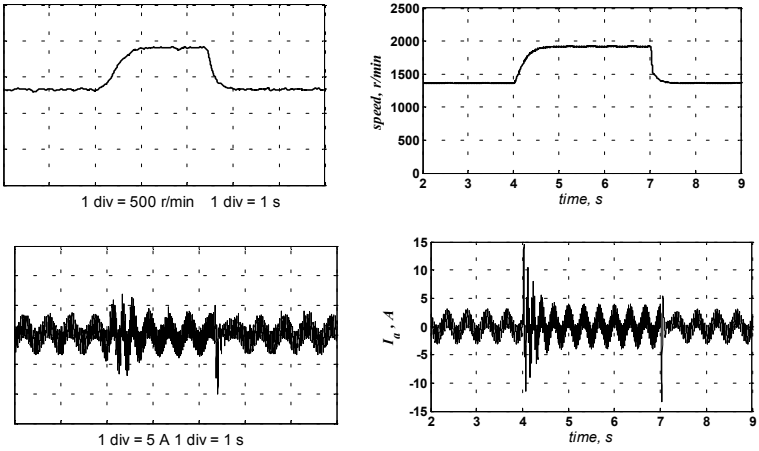


Figure 9: Speed (upper) and current (lower) response to change in frequency from 25 Hz to 35 Hz then to 25 Hz for $f_b$ =50 Hz at no-load.

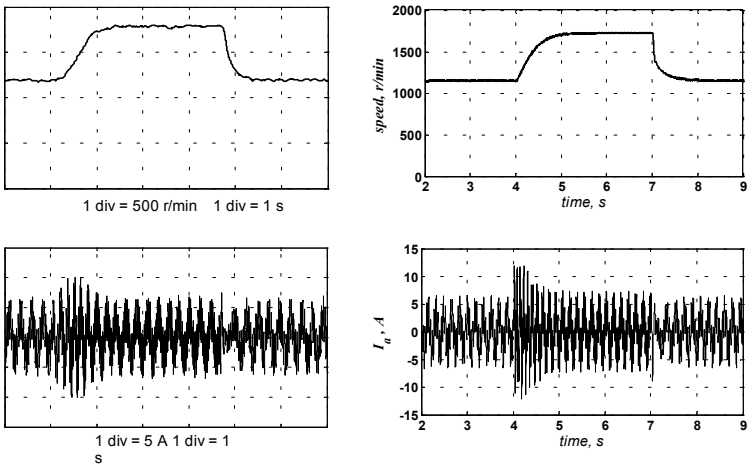


Figure 10: Speed (upper) and current (lower) response to change in frequency from 25 Hz to 35 Hz then to 25 Hz for $f_b$ =50 Hz at load torque of 3 Nm.

## 4. STABILITY ANALYSIS

To study the reasons of instability when operating in the high-speed mode, the dynamic model given by (1, 3 and 4) has been linearized near a given operating point. The standard state-space form of the linearized model is given by:

$$p\mathbf{x} = \mathbf{A}\mathbf{x} + \mathbf{B}\mathbf{u} \tag{5}$$

where; $\mathbf{x} = \left[\Delta i_d \quad \Delta i_q \quad \Delta\omega_m \quad \Delta\delta\right]^T$,

$$\mathbf{A} = \begin{bmatrix} -\frac{R_a}{L_d} & \left(\frac{P}{4}\right)\omega_{mo}\frac{L_q}{L_d} & \left(\frac{P}{4}\right)i_{qo}\frac{L_q}{L_d} & \frac{V_m \cos\delta_o}{L_d} \\ -\left(\frac{P}{4}\right)\omega_{mo}\frac{L_d}{L_q} & -\frac{R_a}{L_q} & -\left(\frac{P}{4}\right)i_{do}\frac{L_d}{L_q} & -\frac{V_m \sin\delta_o}{L_q} \\ i_{qo}\frac{K_t}{J_m} & i_{do}\frac{K_t}{J_m} & -\frac{B_m}{J_m} & 0 \\ 0 & 0 & \left(\frac{P}{4}\right) & 0 \end{bmatrix},$$

$\mathbf{B} = \left[0 \quad 0 \quad -1/J_m \quad 0\right]^T$, $u = \Delta T_L$ and $K_t = \frac{3}{2}\frac{P}{4}\left(L_d - L_q\right)$.

The subscript 'o' in $i_{do}$, $i_{qo}$, $\omega_{mo}$ and $\delta_o$ stands for the steady state quantities of $i_d$, $i_q$, $\omega_m$ and $\delta$, respectively, before application of the small disturbance.

### 4.1 Effect of supply frequency

Table I shows variation of system eigenvalues $\lambda_1, \lambda_2, \lambda_3$ and $\lambda_4$ at no-load for different $V_s/f_s$ patterns. The results are given for $f_s$ range from 15 Hz up to near a maximum value defined by the torque capability limit of the motor for the given $V_s/f_s$ pattern as shown in Figure 11. This limit is in the constant $V_s$ (flux weakening) range, where torque decreases with the increase in frequency. Beyond this frequency limit, maximum toque $T_{Lmax}$ is less than that required by the load and friction. It is to be noted that torque decreases with the increase in base frequency $f_b$. This is owed to the reduction in flux due to the decrease in $V_s/f_s$ ratio with increase in $f_b$ as shown in Figure 1.

The roots $\lambda_1, \lambda_2$ are associated with the electrical system ($i_d$ and $i_q$ respectively) while $\lambda_3, \lambda_4$ are associated with the mechanical system ($\omega_m$ and $\delta$, respectively).

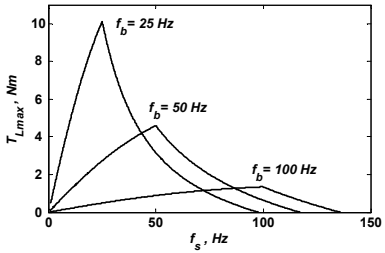


Figure 11: Variation of maximum load torque $T_{Lmax}$ with frequency for the different $V_s/f_s$ patterns.

From Table I, it is noted that instability is associated with eigenvalues $\lambda_3$ and $\lambda_4$, while $\lambda_1$ and $\lambda_2$ are relatively far in the left side of complex plane. Therefore, interest will be given to $\lambda_3$ and $\lambda_4$. Another note is obvious from Table I; the motor is unstable all over most of the given range of frequencies. The real parts of $\lambda_3$ and $\lambda_4$ decrease with increase in $f_s$. Stable operation is only possible in a small range of frequencies in the flux-weakening region Moreover, for $f_b$ = 100 Hz, the stable operation is not possible within $f_s$ range defined by Figure 11.

Table I: Variation of eigenvalues at no-load for different frequencies and V/F patterns.

| $f_b$, *Hz* | $f_s$ *Hz* | $\lambda_1, \lambda_2$ | $\lambda_3, \lambda_4$ |
|---|---|---|---|
| **25** | 15 | - 80.5 ± *j* 76.71 | + 8.38 ± *j* 35.51 |
| for $f_s \leq 25$ Hz | 25 | - 76.9 ± *j* 143.64 | + 4.83 ± *j* 41.2 |
| $V_s/f_s = 2*(V_s/f_s)_{rate}$ | 50 | - 72.4 ± *j* 306.28 | + 0.28 ± *j* 21.0 |
| else | 75 | - 72.1 ± *j* 465.98 | + 0.02 ± *j* 12.96 |
| $V_s=(V_s)_{base}$ | 95 | - 72.1 ± j 592.75 | - 0.02 ± *j* 6.57 |
| **50** | 15 | - 243.5 & - 56.7 | + 5.99 ± *j* 23.19 |
| | 25 | - 148.1 ± *j* 78.84 | + 3.97 ± *j* 27.66 |
| for $f_s \leq 50$ Hz | 50 | - 145.3 ± *j* 281.6 | + 1.2 ± *j* 29.54 |
| $V_s/f_s = 2*(V_s/f_s)_{rate}$ | 75 | - 144.3 ± *j* 449.9 | + 0.19 ± *j* 18.95 |
| else | 100 | - 144.1 ± *j* 612.4 | + 0.03 ± *j* 12.38 |
| $V_s=(V_s)_{base}$ | 115 | - 144.1 ± *j* 708.8 | - 0.01 ± *j* 6.7 |
| **100** | 15 | - 552.4 & -30.4 | + 3.20 ± *j* 13.57 |
| | 25 | - 520.5 & -60.8 | + 2.51 ± *j* 16.71 |
| for $f_s \leq 100$ Hz | 50 | - 289.1 ± *j* 142.1 | + 0.91 ± *j* 18.58 |
| $V_s/f_s = ½ (V_s/f_s)_{rated}$ | 75 | - 288.6 ± *j* 378.5 | + 0.41 ± *j* 18.77 |
| else | 100 | - 288.4 ± *j* 562.02 | + 0.22 ± *j* 18.7 |
| $V_s=(V_s)_{base}$ | 125 | - 288.2 ± *j* 733.37 | + 0.04 ± *j* 11.85 |

For loaded cases, the stability matter becomes worst, even in flux weakening range. To clarify this point, Figure 12a shows the $\lambda_3$ (the root of positive imaginary part) locus plot for different loads for $f_s$ range from 15 Hz (right end of a curve) up to maximum values as discussed before and given by Figure 11. The break point of a curve corresponds to $f_s=f_b$ , i.e. the transition from constant $V_s/f_s$ to constant $V_s$. Figure 12b shows the variation of the real part of $\lambda_3$ and $\lambda_4$ with $f_s$ near the stable range.

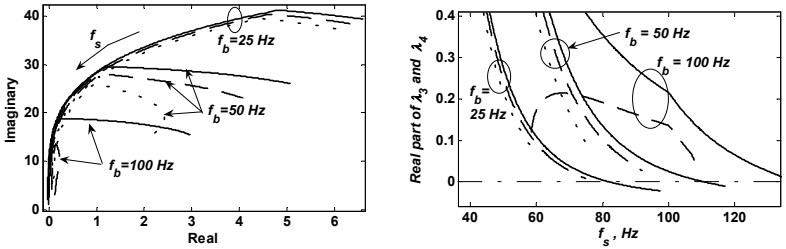


Figure 12: Effect of varying $f_s$ on the motor stability for different values of load and base frequency: $T_L$=0 (solid lines), $T_L$ = 1 Nm (dashed lines), $T_L$ = 2 Nm (dotted lines). a) $\lambda_3$ locus plot for $f_s$ range from 15 Hz (right end of a curve) up to maximum values at different loads, b) Variation of real part of $\lambda_3$ and $\lambda_4$ near the stable range.

The results given in Table I and figure 12 justify the experimental instability of the adopted motor in the high-speed mode. Therefore, the effect of motor parameters has to be checked to find out how to design a stable motor to operate in such a mode. With the aid of the previous work, it has been proved that the most effective parameter is the rotor-to-stator turns ratio *K*. It was found that the machine capabilities increase with the increase in *K*, either for the generator mode [7] or motor operating at low speed mode [3]. This note has encouraged giving attention to that parameter.

### 4.2 Effect of rotor-to-stator turns ratio

It has been assumed that changing of turns ratio is achieved by varying the rotor number of turns while the stator winding is kept unchanged. The effect of varying turns ratio on the other parameters such as resistance $R_a$, leakage and mutual inductances ($L_r$ and $M$) has been considered as described in detail in [3].

Therefore, varying turns ratio from a base value of $K_b$ to a new value $K$ results in a variation of rotor resistance, rotor leakage inductance and magnetizing inductance to be:

$$\left.\begin{aligned} R_{an} &= R_{ab}\left(K/K_b\right)^2 \\ L_{rn} &= L_{rb}\left(K/K_b\right)^2 \\ M_n &= M_r\left(K/K_b\right) \end{aligned}\right\} \qquad (6)$$

where subscript ‘b’ stands for base value of the employed machine, and ‘n’ for the new values.

The base value has been assumed to be that of the given motor. It is very close to unity (1.005) so that a new value can be considered as the per unit value.

Figure 13 shows variation of real part of $\lambda_3$ and $\lambda_4$ with $f_s$ for different turns ratio $K$ at $f_b$=50 Hz and no-load. For each case, upper limit of $f_s$ is determined by the torque capability limit of the motor for the given *V/f* pattern, which is shown in Figure 14. As attained before [3 & 7], the torque capability of SCIM in high-speed operation is maximum when $K$=1. It is noted from Figure 14 that torque capability drops more sharply for $K$>1 compared with cases of $K$<1. For example compare the curve of $K$=0.5 with that of $K$=2. That can be attributed to the increase in winding resistance and leakage inductance for $K$>1, which result in an increase in voltage drop. Therefore cases of K>1 is not practically feasible.

Important notes can be obtained from Figure 13 and 14. For higher values of $K$, the stable range of $f_s$ decreases. For example, when $K$=1, the operation is stable when 112Hz < $f_s$<118 Hz. The lower limit is determined by the stability analysis as shown in Figure 13, while the upper limit is determined by the torque capability as shown in Figure 14. Similarly, stable range of $f_s$ can be obtained for a given value of $K$.

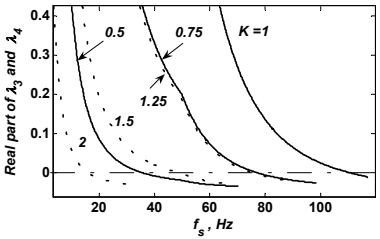


Figure 13: Variation of real part of $\lambda_3, \lambda_4$ with $f_s$ for different turns ratio $K$ at $f_b$=50 Hz at no-load (dashed lines are for K>1).

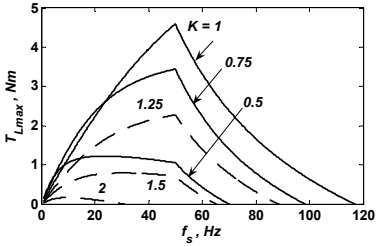


Figure 14 Variation of maximum load torque $T_{Lmax}$ with frequency for different turns ratio $K$ at $f_b$=50 Hz (dashed lines are for K>1)

Figure 15 shows the stability and operation limits of SCIM for different loads. It is noted from Figs. 15a and b, that the stable range of $f_s$ decreases with loading. Figures 15c and d shows the relations for higher loads. Emphasis is given to the range of $K$<1.

From the previous discussion it is clear that the advantage of high torque capability for higher values of $K$ is limited by the associated low stability. One of the instability sources is the absence of inherent damping as provided, for example, by cage windings in some types of motors. Moreover, the given results show the great effect of $K$ on the stability. Therefore, it was not possible to attain a stable operation using the adopted experimental motor whish has $K$=1.005. Moreover, it was possible, with difficulties, to get results given in [4] for a motor of $K$=0.68. Accordingly, the stable operation of SCIM in high-

speed mode is expected not to be satisfactory unless a suitable control system is integrated with the motor in a drive system as presented in [6] for a motor of $K$=0.5. Effect of $K$ on the control system design becomes now an important topic for research.

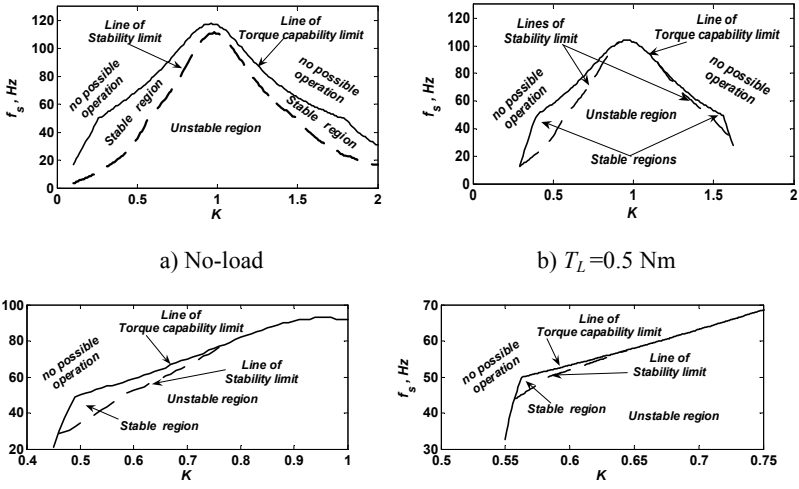


a) No-load b) $T_L$=0.5 Nm

c) $T_L$=1 Nm d) $T_L$=1.5 Nm

Figure 15: Operation and Stability Limits for $f_b$=50 Hz

## 5. CONCLUSION

The dynamic behavior of SCIM has been analyzed and investigated in this paper. The operation in both low- and high-speed modes is considered. Effect of varying supply voltage and frequency under V/f scalar control technique has been investigated. Experimental and simulation results show possible operation at low speed mode, while attaining high-speed mode was not possible. For low-speed mode, the dynamic behavior is similar to that obtained when applying *V/f* control technique to the conventional motor types. A main difference is the presence of sub harmonic current component at slip frequency, which is a known feature of SCIM operation in low-speed mode.

To investigate how to achieve operation at high-speed mode, stability analysis based on a linear model has been carried out. It was found that stable operation of the adopted motor is only possible in a small range of frequencies in the flux-weakening region especially for loaded cases. Therefore, the effect of motor parameters has been studied to obtain a useful design guide. It was found that rotor-to-stator turns ratio plays an important role in the motor stability. Torque capability of the motor increases with increasing that ratio. However,

this capability is associated with a decrease in stable range of operation. Low stability is owed to the absence of inherent damping as provided, for example, by cage windings in some types of motors. This means that stable operation of SCIM in high-speed mode is expected not to be satisfactory unless it is integrated with a suitable control system. Effect of turns ratio on the control system design has to be studied in order to get the benefits of motors of high ratio.

**Acknowledgment**

The author gratefully acknowledges the sincere help of his colleagues: Eng. Mohamed Abou El-Azm and Eng. Wael El-Awady in preparing the digital recording system used to get the experimental results.

## REFERENCES

[1] A. S. Mostafa, A. L. Mohamadein and E. M. Rashad, "Analysis of series - connected wound-rotor self-excited induction generator", *IEE Proc. B*, Vol. 140, No. 5, Sept. 1993, pp. 329-336.

[2] E. M. Rashad, "Sub-synchronous operation of the three-phase parametric motor", in *Proc. of 33rd Universities Power Engineering Conference, UPEC'98, Sept. 1998, Napier University, Edinburgh, UK*, pp 608-611.

[3] E. M. Rashad, "Feasibility of operating the parametric motor in the Sub-Synchronous Mode", *Engineering Research Bulletin, Faculty of Engineering, Menoufiya University. Egypt*, vol. 22 No. 2, July 1999, pp165-189.

[4] E. M. Rashad, M. E. Abdel-Karim, and Y. G. Desouky, "Theory and analysis of three phase series-connected parametric motors", *IEEE Trans. Energy Conversion*, vol. 11 No. 4 pp 715-720, Dec. 1996.

[5] M. A. Badr, A. I. Alolah and A. F. Almarshood, "Transient performance of series-connected three-phase slip-ring induction motors", *IEEE Trans. Energy Conversion*, vol. 13, No. 4, pp 305-310, Dec. 1998

[6] E. M. Rashad, T. S. Radwan and M. A. Rahman, "Starting and Vector Control of Series-Connected Wound-Rotor Induction Motor in Super Synchronous Mode", *in Proc. of the 39th IEEE Industry Application Society Annual Meeting* held in Seattle, Washington from 2 to 7 Oct. 2004, Vol. I, pp 32-39.

[7] A. L. Mohamadein, and E. A. Shehata, "Theory and performance of series-connected wound-rotor self-excited synchronous generators", *IEEE Trans. Energy Conversion*, vol. 10, No. 3, pp 508-515, Sept. 1995.

## Nomenclature

| | |
|---|---|
| $f_s$ | Supply frequency, Hz |
| $i_d$ & $i_q$ | transformed *d*- & *q*-axis currents, respectively, A |

| | |
|---|---|
| $I_a$ | Phase rms motor current, A |
| K | Rotor to stator effective turns ratio. |
| $L_s$ & $L_r$ | Stator & rotor leakage inductances respectively, H |
| $M$ | Maximum mutual inductance between one stator phase and one rotor phase, H |
| $P$ | Number of poles. |
| $R_s$ & $R_r$ | Stator & rotor phase resistances respectively, □. |
| $T_e$ | Electromagnetic developed torque, Nm. |
| $T_L$ | Mechanical load torque, Nm. |
| $v_d$ & $v_q$ | transformed *d*- & *q*- axis voltages, respectively, V |
| $V_m$ & $V_s$ | Maximum and rms values of supply voltage, respectively, V |
| $\delta$ | Angle between supply voltage phasor and q-axis (Load angle), electrical rad |
| $\omega_m$ | Rotor speed, mechanical rad/s |

## Appendix

The adopted two-pole wound-rotor induction motor in this paper has the following nameplate data:

1.1 KW, 380/220 V, Y/ Δ , 2.5/4.3A, 50 Hz.

The measured parameters of the motor (using conventional tests of induction motors) are as given in the following table:

| Parameter | Measured value ( Ω /phase) |
|---|---|
| Stator winding dc resistance $R_{sdc}$ | 4.5 |
| Rotor winding dc resistance $R_{rdc}$ | 4.33 |
| Stator leakage reactance $X_s$ (at 50 Hz) | 4.87 |
| Rotor leakage reactance (referred to the stator side) $X'_r$ (at 50 Hz) | 4.87 |
| Magnetizing reactance $X_m$ (at 50 Hz) | 198.36 |
| Stator to rotor turns ratio | $K$ = 1.005 |